Electronic Supplementary Material (ESI) for Energy & Environmental Science

Supplementary information for "Charge transport in lithium peroxide: relevance for rechargeable metal-air batteries"

Maxwell D. Radin[†], Donald J. Siegel*[,‡]

[†]Department of Physics, University of Michigan, Ann Arbor, Michigan 48109, United States

[‡]Department of Mechanical Engineering, University of Michigan, Ann Arbor, Michigan 48109, United States

*E-mail: djsiege@umich.edu

Defects

Table S1 shows the calculated equilibrium formation energies for all defects studied using both PBE GGA and HSE hybrid functionals. Geometries were fully relaxed with each functional. Charge states of -1, 0, and +1 were considered for all defect types. In cases where chemical intuition suggested that other charge states might be reasonable, we included additional possibilities. Given that oxygen atoms occur as covalently bonded dimers, we also considered oxygen divacancies (V_{O2}) in which an entire O_2 unit is removed. The initial guess used for the hole polaron geometry was created by shortening the O-O bond length by 10% and moving the nine nearest Li sites away from the O-O midpoint; six of the nine were moved 5% further away and three were moved 4%. The initial guess for electron polarons simply consisted of a 20%

increase in the O-O bond length. While not included in the table below, we did consider hole bipolarons, p^{2+}. However, we were not able to localize both holes at a single O_2 dimer. Seven interstitial sites were considered: centers of empty prisms, centers of tetrahedra, centers of faces shared by prisms and octahedra, sides of prisms, centers of faces shared by tetrahedra and prisms, centers of faces shared by octahedra and tetrahedra, and off-center of empty prisms (displaced halfway towards a corner). GGA calculations were performed at all seven sites for all charge states considered; hybrid calculations were done using only the site predicted to be lowest in energy by GGA for a given charge state. For all charge states, oxygen interstitials were found to favor the site off-center of empty prisms, forming a structure that resembles an ozonide ion. Neutral lithium interstitials also favored this site, while the negative and positive lithium interstitials favored the faces of octahedra/tetrahedra and centers of empty prisms, respectively.

Figure S1 shows the magnetization density of the hole polaron. The distribution of the magnetization density represents the location of the hole. As α goes from 0 to 0.25 to 0.48, the hole becomes more localized.

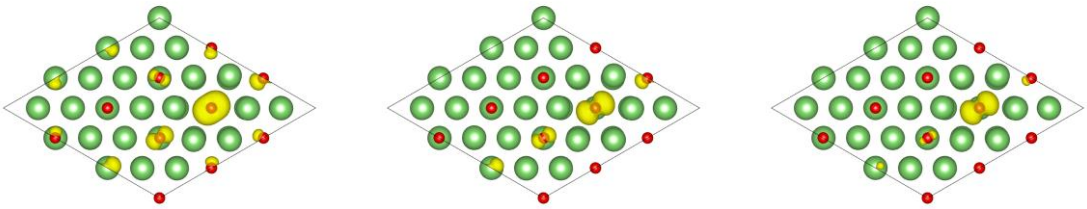

(a) GGA (b) HSE (α = 0.25) (c) HSE (α = 0.48)

Figure S1. Magnetization density isosurface of the hole polaron calculated with (a) PBE, (b) HSE (α = 0.25), and (c) HSE (α = 0.48). All three calculations shown here were performed at the α = 0.25 geometry. The polaron is viewed from along the c axis.

Table S1. Equilibrium defect formation energies (eV) and concentrations (cm^{-3}) for all defects examined.

	GGA	HSE (α = 0.25)	HSE (α = 0.48)
p^{2-}	2.38 (3×10^{-18})	3.20 (6×10^{-32})	3.12 (1×10^{-30})
p^{-}	0.91 (1×10^{7})	1.44 (2×10^{-2})	1.51 (1×10^{-3})
p^{+}	–	0.85 (5×10^{8})	0.95 (1×10^{7})
V_{Li}^{-} (O)	0.36 (3×10^{16})	0.87 (8×10^{7})	0.95 (3×10^{6})
V_{Li}^{-} (TP)	0.29 (4×10^{17})	0.83 (4×10^{8})	0.93 (7×10^{6})
V_{Li}^{0} (O)	0.37 (2×10^{16})	1.20 (2×10^{2})	1.37 (4×10^{-1})
V_{Li}^{0} (TP)	0.22 (6×10^{18})	0.86 (1×10^{8})	1.02 (2×10^{5})
V_{Li}^{+} (O)	0.81 (9×10^{8})	1.82 (9×10^{-9})	2.05 (1×10^{-12})
V_{Li}^{+} (TP)	0.59 (4×10^{12})	1.23 (7×10^{1})	1.45 (1×10^{-2})
V_{O}^{-}	2.54 (1×10^{-20})	3.27 (8×10^{-33})	3.58 (4×10^{-38})
V_{O}^{0}	0.73 (3×10^{10})	0.74 (2×10^{10})	0.74 (2×10^{10})
V_{O}^{+}	1.16 (2×10^{3})	1.57 (3×10^{-4})	1.66 (9×10^{-6})
V_{O2}^{-}	1.81 (1×10^{-8})	2.38 (4×10^{-18})	2.47 (1×10^{-19})
V_{O2}^{0}	4.42 (2×10^{-52})	4.62 (7×10^{-56})	4.71 (2×10^{-57})
V_{O2}^{+}	4.70 (3×10^{-57})	4.34 (5×10^{-51})	4.32 (1×10^{-50})
V_{O2}^{2+}	4.24 (2×10^{-49})	3.35 (2×10^{-34})	3.24 (9×10^{-33})
O_{i}^{2-}	3.38 (2×10^{-34})	4.44 (3×10^{-52})	4.55 (4×10^{-54})
O_{i}^{-}	2.79 (1×10^{-24})	4.07 (5×10^{-46})	4.34 (1×10^{-50})
O_{i}^{0}	1.37 (8×10^{-1})	1.37 (8×10^{-1})	1.33 (5×10^{0})
O_{i}^{+}	1.70 (3×10^{-6})	2.20 (1×10^{-14})	2.22 (5×10^{-15})
Li_{i}^{-}	3.39 (1×10^{-34})	3.83 (4×10^{-42})	3.80 (1×10^{-41})
Li_{i}^{0}	2.65 (3×10^{-22})	2.59 (3×10^{-21})	2.51 (6×10^{-20})
Li_{i}^{+}	2.40 (1×10^{-18})	1.83 (5×10^{-9})	1.69 (1×10^{-6})

GW Convergence Tests

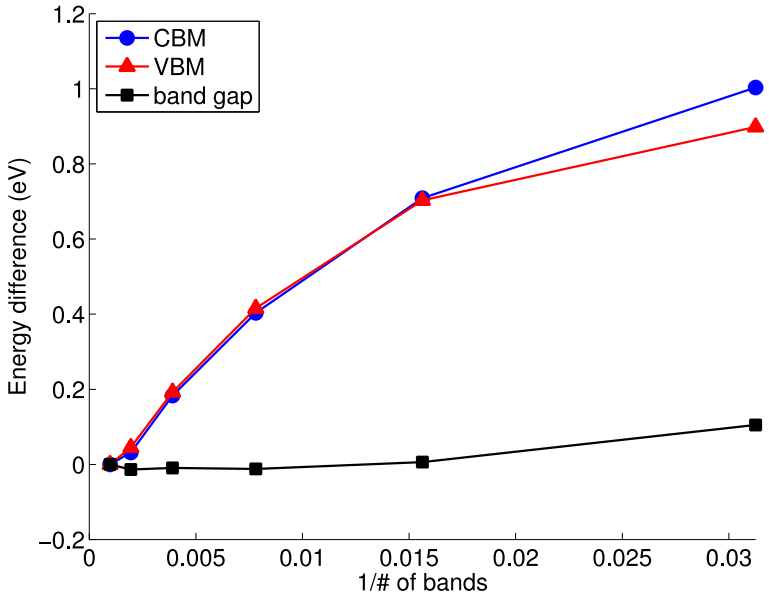

Figure S2. Convergence of the GGA+G_0W_0 band edges and band gap with respect to the number of bands used in the calculation. Data shown for calculations on a conventional unit cell with a number of bands equal to 32, 64, 128, 256, 512, and 1024. Based on this data, we chose to use 1024 bands. An extrapolation to an infinite number of bands indicates that the band edges are converged to within about 50 meV.

Hopping and Migration Pathways

All five nearest neighbor V_{Li}^{-} migration pathways were considered. The GGA nudged elastic band energy barriers for these paths are listed in Table S2 (see also Figure S3). For the A→ D pathway, two values are given because the TP and O sites have slightly different energies.

Table S1. Migration barriers for V_{Li}^{-} migration calculated using the nudged elastic band method at the GGA level of theory.

Path	Barrier (eV)	Description
A→B	1.00	In-plane between TP sites.
C→ D	1.06	In-plane between O sites.
A→E	2.34	Out-of-plane between TP sites.
D→F	1.60	Out-of-plane between O sites.
A→ D	0.39/0.33	Between TP and O sites.

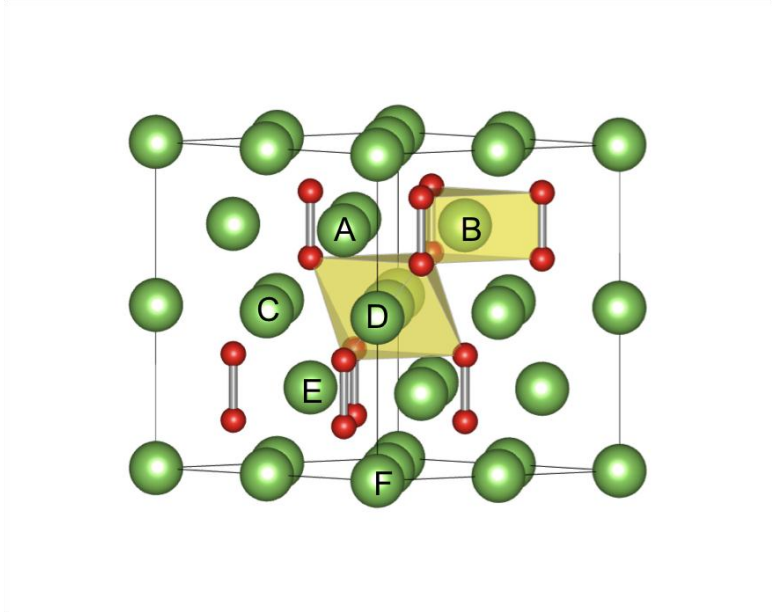

Figure S3. Lithium vacancy migration pathways.

Similarly, all nearest-neighbor hole polaron hopping pathways were considered. The O_2 dimers form a distorted hcp lattice in Li_2O_2. Neglecting the Jahn-Teller distortion of the hole polaron, there would be six symmetry equivalent in-plane nearest-neighbor hopping paths and six symmetry equivalent out-of-plane nearest-neighbor hopping paths. The Jahn-Teller distortion allows for three possible orientations of the initial and final states, so in principle there are 3 × 3

= 9 possible hopping paths between any two sites. However, several of these paths are symmetry equivalent. For in-plane hopping, there are only six symmetry inequivalent paths, and for out-of-plane hopping there are only four. Figure S4 summarizes these paths graphically and gives the calculated HSE barriers (α = 0.48) based on a linear interpolation of images. Additionally, there is a trivial in-place rotation path, for which we find an barrier of 5 meV.

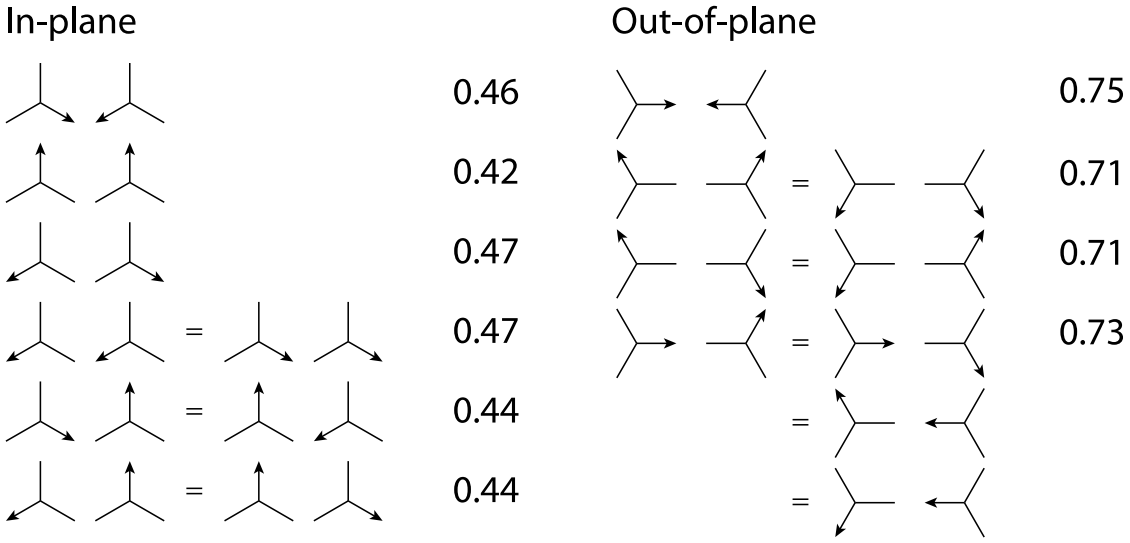

Figure S4. Nearest neighbor hole polaron hopping paths. Each path is depicted by two glyphs which represent the initial and final polaron states. The three lines represent the directions of three nearest trigonal prismatic Li sites. The arrow indicates the direction of the Jahn-Teller distortion (i.e. which of the three O-Li bonds is contracted). The hopping direction is left to right, and symmetry equivalent paths are indicated by an equals sign. Hopping barriers calculated from a linear interpolation of images are given in eV.

Estimation of target conductivity

We estimate the conductivity required for a hypothetical bipolar plate battery pack described by Adams and Karulkar.[1] We assume that the cathode uses carbon with a specific area of 100 m^2/g_C,[2] and that Li_2O_2 forms a film of uniform thickness. Based on the parameters shown in

Table S2, the film will be of thickness $T = QV/4ae = 6$ nm, where e is the elementary charge and the factor of four arises from the fact that four electrons are transferred per unit cell of Li_2O_2. The carbon loading is $L = E/NAUQ = 0.013\ g_C/cm^2$, so the microscopic current density is $j = i/aL = 3.4\ \mu A/cm^2$. To achieve an iR drop across the discharge product of $\eta = 0.1$ V, the conductivity must be $\sigma = Tj/\eta = 2 \times 10^{-11}$ S/cm. We assume an uncertainty of two orders of magnitude in this estimate.

Table S2. Parameters used to determine overpotential for a hypothetical Li-air battery.

Parameter	Description	Units	Value
Q	Specific capacity	C/g_C	1650
$\boldsymbol{E}$	Pack energy	Wh	40
$\boldsymbol{N}$	Number of cells	Dimensionless	1434
$\boldsymbol{i}$	Macroscopic current density	mA/cm^2	42
A	Plate active area	cm^2	500
U	Cell voltage	V	2.7
V	Li_2O_2 unit cell volume	$Å^3$	64
a	Specific area of carbon	m^2/g_C	100

Computational Methods

First principles calculations were performed using the Vienna *ab initio* simulation package (VASP),[3–6] with Blöchl's projector augmented wave (PAW) method,[7] 2s and 2s2p electrons treated as valence for Li and O, and a plane-wave cutoff energy of 400 eV. Occupancies were determined with a Gaussian smearing of width 0.1 eV for bulk phases and 0.01 eV for molecules. Lattice constants were determined by relaxing the cell shape, volume, and atomic positions of the conventional unit cells. All atomic forces were minimized to a tolerance of 0.02 eV/Å, with the cell shape/volume held constant during defect calculations. A 3×3×2 supercell (144 atoms) with Γ-point k-space integration was used for defect calculations. All calculations

used the lattice constants obtained with α = 0.25 (a = 3.12 Å and c = 7.61 Å). Since there has been no experimental measurement of the bandgap, we fit the mixing parameter α to the average of the GGA+G_0W_0 and GGA+scGW band gaps (calculated at the α = 0.25 geometry); this choice is motivated by the fact that GGA+G_0W_0 is known to underestimate gaps, while GGA+scGW (in the absence of vertex corrections) overestimates gaps.[8,9] We obtained GGA+G_0W_0 and GGA+scGW gaps of 7.76 and 5.70 eV; the 36% difference between the these two values is not uncommon.[8,9] We found that a mixing parameter of α = 0.48 reproduces the reference gap of 6.62 eV. Given the uncertainty in the true band gap, there is some uncertainty in the optimal value of α and therefore the polaron hopping barrier (and, to a lesser extent, defect formation energies). (Additionally the value of α that reproduces the true band gap may not exactly reproduce the true band edges nor the hopping barrier.[10]) A higher level of theory may be needed to further refine our estimate of the polaron hopping barrier.

The equilibrium concentration C of a defect X in charge state q in a given solid phase can be written as $C(X^q) = D_X e^{-E_f(X^q)/k_B T}$, where D_X is the number density of defect sites.[11] The formation energy E_f is calculated as:[12]

$$E_f(X^q) = E_0(X^q) - E_0(\text{bulk}) - \sum_i n_i \mu_i + q\varepsilon_F + E_{MP1}$$

where n_i is the number of atoms of the i^{th} species in the defect, μ_i is the chemical potential of that species, ε_F is the Fermi level, and E_{MP1} is the Makov-Payne monopsize correction.[13,12]

We set the chemical potential of oxygen to be one half the free energy of gaseous O_2 at 300 K and 0.1 MPa; This condition captures a scenario under which the cathode and the electrolyte (including dissolved oxygen) are in equilibrium with oxygen in the air. We calculate the free energy of oxygen as

$$G(300\text{ K}, O_2) = E_0(O_2) + k_b T - TS_{expt}$$

where the k_bT term accounts for the pV contribution to free energy, and S_{expt} is the experimental entropy.[14] We have intentionally neglected the small contributions to the free energy due to the translational, rotational, and vibrational degrees of freedom because we are not including these terms in the bulk phases; this maintains some degree of error cancellation. The chemical potential of Li in Li_2O_2 within the cathode may be related to the chemical potential of Li in the anode (BCC Li) via the following expression:[15]

$$\mu_{\text{Li}}(\text{cathode}) = \mu_{\text{Li}}(\text{BCC Li}) - eE$$

where e is the elementary charge and E is the cell potential. Note that the open circuit voltage corresponds to the same thermodynamic boundary condition as isolated Li_2O_2, $\mu_{\text{Li}}^{\text{OCV}} = \frac{1}{2}(G(300\text{ K}, \text{Li}_2\text{O}_2) - 2\mu_{\text{O}})$. The assumption of local thermodynamic equilibrium within the cathode during cell operation ($E \neq E^{\text{OCV}}$) is justified by the facility of lithium kinetics over the length and time scales relevant to cell operation. The predicted V_{Li}^{-} diffusivity[16] is fairly high at 6×10^{-9} cm^2/s, which corresponds to a characteristic diffusion length[16] over one hour ($L = \sqrt{Dt} = 47$ μm) that is much larger than the typical discharge product particle size (1 μm or less[17,18]), and prior experimental and computation studies indicate that the kinetic barrier for lithium adsorption/desorption from a Li_2O_2 surfaces is quite low.[19–21]

Because DFT systematically overbinds gas-phase O_2 relative to solid oxides,[22,23,19] we correct the ground state energy of the O_2 molecule using the experimental formation enthalpy of Li_2O_2. For defect calculations, we apply a correction to the energy of O_2 based on the experimental formation enthalpy of Li_2O_2 at 300 K, $\Delta H_f(\text{Li}_2\text{O}_2)^{\text{expt}} = -6.57$ eV:[14]

$$E_0(\text{O}_2)^{\text{corr}} = E_0(\text{O}_2) + \Delta H_{\text{f}}(\text{Li}_2\text{O}_2)^{\text{calc}} - \Delta H_{\text{f}}(\text{Li}_2\text{O}_2)^{\text{expt}}$$

This increases the energy of O_2 molecule by 0.78, 0.68, and 0.58 eV for α = 0, 0.25, and 0.48. We note that prior studies have found that the error in formation energy varies to some degree

between different alkali and alkaline-earth metal oxides, peroxides, and superoxides.[19] This indicates that in addition to errors in the ground state energy of the O_2 molecule, there is some error associated with the solid phases. However, we note that our results are not greatly sensitive to the choice of correction: a 0.1 eV change in the O_2 correction changes the equilibrium hole polaron formation energy only by only 0.025 eV.

Lastly, we discuss finite-size effects in our simulations. While more complicated finite size corrections have been proposed, the monopole errors have been shown to be the leading error, scaling as one over the length of the supercell.[12] We note that the inclusion of the monopole correction is an improvement over previous studies on polarons in Li_2O_2, which did not include any finite size corrections.[24,25] Using density functional perturbation theory (with the PBE functional),[26] we have calculated the in-plane and out-of-plane relaxed-ion (*i.e.* low-frequency) dielectric constants of Li_2O_2 to be $\varepsilon_{xx} = \varepsilon_{yy} = 7.48$ and $\varepsilon_{zz} = 12.54$; given the relatively modest anisotropy, we simply adopt a value of $\varepsilon = 10$ for the purposes of calculating finite size corrections. This yields a correction of $E_{MP1} = 0.17$ eV for defects with a charge of $q = \pm 1$ in our 3×3×2 supercell.

Figure S5 shows that the MP1 correction significantly improves size convergence for the V_{Li}^- (O) defect. We also performed some finite size tests on the hole polaron, as shown in Figure S6. However, because this defect is unstable in GGA, it was necessary to use a hybrid functional; consequently it was not possible to go to larger cell sizes. At small sizes, one can see that the hole polaron in HSE is more sensitive to supercell size than the negative lithium vacancy. Based on the magnetization density shown in Figure S1(b), we attribute this behavior to wavefunction overlap between periodic images.[27]

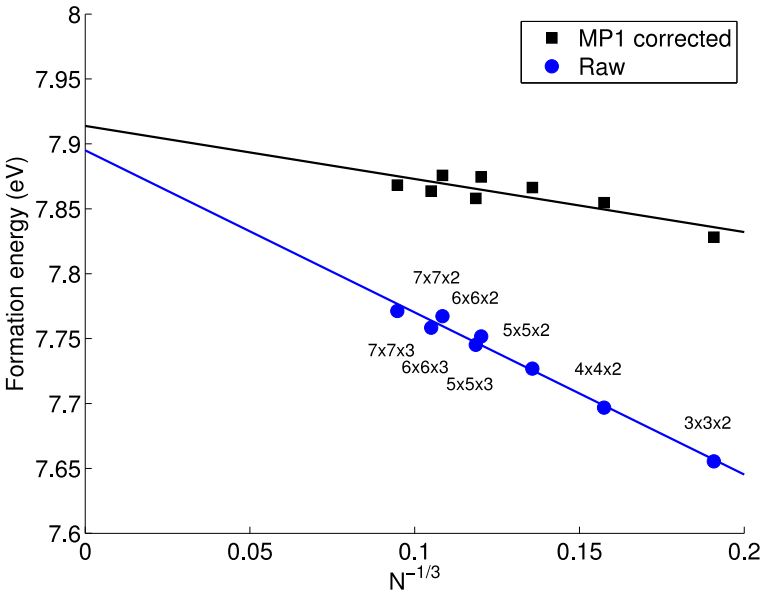

Figure S5. Size convergence of the V_{Li}^{-} (O) GGA formation energy referenced to the average electrostatic potential. Calculations were performed up to a 7 × 7 × 3 supercell (N = 1176 atoms). A linear fit is shown to allow for extrapolation to infinite supercell size.

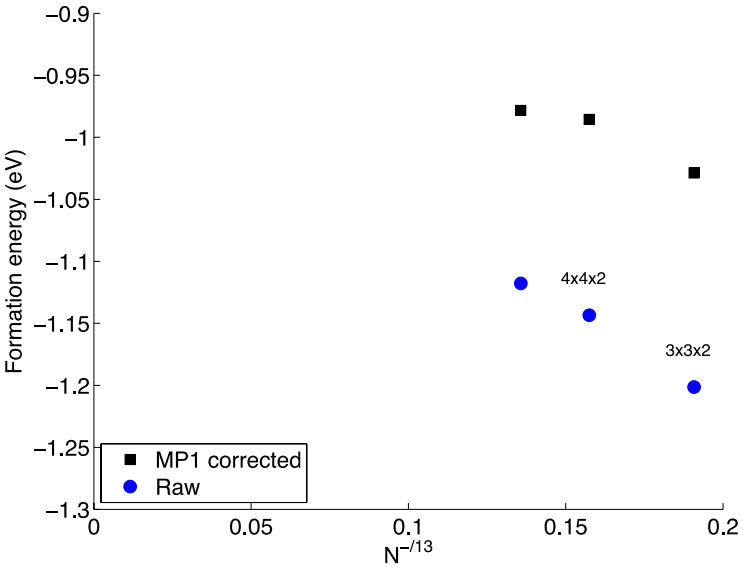

Figure S6. Size convergence of the hole polaron HSE (α = 0.48) formation energy referenced to the average electrostatic potential. Calculations were performed up to a 5 × 5 × 2 supercell (N =

400 atoms). We refrain from including a linear fit because the errors due to wavefunction overlap are not expected to have a linear dependence on the cell dimension.

References

1. J. Adams and M. Karulkar, *J. Power Sources*, 2012, **199**, 247–255.
2. Y.-C. Lu and Y. Shao-Horn, *J. Phys. Chem. Lett.*, 2013, **4**, 93–99.
3. G. Kresse and J. Hafner, *Phys. Rev. B*, 1994, **49**, 14251–14269.
4. G. Kresse and J. Furthmüller, *Phys. Rev. B*, 1996, **54**, 11169–11186.
5. G. Kresse and J. Furthmüller, *Comput. Mater. Sci.*, 1996, **6**, 15–50.
6. G. Kresse and J. Hafner, *Phys. Rev. B*, 1993, **47**, 558–561.
7. P. E. Blöchl, *Phys. Rev. B*, 1994, **50**, 17953.
8. M. Shishkin and G. Kresse, *Phys. Rev. B*, 2007, **75**, 1–9.
9. M. Shishkin, M. Marsman, and G. Kresse, *Phys. Rev. Lett.*, 2007, **99**, 246403.
10. A. Alkauskas, P. Broqvist, and A. Pasquarello, *Phys. Status Solidi B*, 2011, **248**, 775–789.
11. C. G. Van de Walle, *J. Appl. Phys.*, 2004, **95**, 3851.
12. H.-P. Komsa, T. Rantala, and A. Pasquarello, *Phys. Rev. B*, 2012, **86**, 045112.
13. M. C. Payne and G. Makov, *Phys. Rev. B*, 1995, **51**, 4014–4022.
14. M. W. Chase Jr., *Journal of Physical and Chemical Reference Data*, 1998.
15. J. S. Hummelshøj, J. Blomqvist, S. Datta, T. Vegge, J. Rossmeisl, K. S. Thygesen, A. C. Luntz, K. W. Jacobsen, and J. K. Nørskov, *J. Chem. Phys.*, 2010, **132**, 071101.
16. R. J. D. Tilley, *Defects in Solids*, John Wiley & Sons, Inc., 2008.
17. Y.-C. Lu, B. M. Gallant, D. G. Kwabi, J. R. Harding, R. R. Mitchell, M. S. Whittingham, and Y. Shao-Horn, *Energy Environ. Sci.*, 2013, DOI: 10.1039/C3EE23966G.
18. A. Kraytsberg and Y. Ein-Eli, *Nano Energy*, 2012, DOI: 10.1016/j.nanoen.2012.11.016.

19. J. S. Hummelshøj, a C. Luntz, and J. K. Nørskov, *J. Chem. Phys.*, 2013, **138**, 034703.

20. Y. Mo, S. Ong, and G. Ceder, *Phys. Rev. B*, 2011, **84**, 205446.

21. V. Viswanathan, J. K. Nørskov, A. Speidel, R. Scheffler, S. Gowda, and A. C. Luntz, *J. Phys. Chem. Lett.*, 2013, **4**, 556–560.

22. L. Wang, T. Maxisch, and G. Ceder, *Phys. Rev. B*, 2006, **73**, 195107.

23. S. Kurth, J. P. Perdew, and P. Blaha, *Int. J. Quantum Chem.*, 1999, **75**, 889.

24. S. P. Ong, Y. Mo, and G. Ceder, *Phys. Rev. B*, 2012, **85**, 081105.

25. J. Kang, Y. S. Jung, S.-H. Wei, and A. Dillon, *Phys. Rev. B*, 2012, **85**, 035210.

26. X. Wu, D. Vanderbilt, and D. Hamann, *Phys. Rev. B*, 2005, **72**, 035105.

27. S. E. Taylor and F. Bruneval, *Phys. Rev. B*, 2011, **84**, 075155.